



Impact of cyclic mechanical compression on the electrical contact resistance between the gas diffusion layer and the bipolar plate of a polymer electrolyte membrane fuel cell

Khadidja Bouziane ^{a, b, c, d, *}, El Mahdi Khetabi ^{a, b, c, d}, Rémy Lachat ^{c, d, e}, Nada Zamel ^f, Yann Meyer ^{b, c}, Denis Candusso ^{a, d}

^a Université Paris-Saclay, ENS Paris-Saclay, CNRS, Université Gustave Eiffel, SATIE (Systèmes et Applications des Technologies de l'Information et de l'Energie), 94235, Cachan, France

^b Sorbonne Universités, Université de Technologie de Compiègne, CNRS, FRE 2012 Roberval, centre de recherche Royallieu, CS 60 319, 60203, Compiègne cedex, France

^c Univ. Bourgogne Franche-Comté, UTBM bât. F, Rue Thierry Mieg, 90010, Belfort Cedex, France

^d FR FCLAB (FR CNRS 3539), Plateforme pile à combustible, UTBM bât. F, Rue Thierry Mieg, 90010, Belfort Cedex, France

^e ICB (UMR 6303), CNRS Univ. Bourgogne Franche-Comté, UTBM, Belfort, France

^f Fraunhofer Institute for Solar Energy Systems ISE, Freiburg, Germany

ARTICLE INFO

Article history:

Received 29 October 2019

Received in revised form

29 January 2020

Accepted 10 February 2020

Available online 11 February 2020

Keywords:

Fuel cell

Gas diffusion layer

Bipolar plate

Electrical contact resistance

Cyclic compression

ABSTRACT

The electrical contact resistance between the Gas Diffusion Layer (GDL) and the BiPolar Plate (BPP) used in Polymer Electrolyte Membrane Fuel cells (PEMFCs) is responsible for a substantial amount of Ohmic losses in the electrical power generator. This contact resistance was measured for a variety of carbon paper GDLs under cyclic mechanical compression between 0 and 8 MPa according to the Transmission Line Method (TLM). Contact resistance and strain hysteresis were noticed as a result of cyclic compression. The effect of GDL structure and composition on the electrical contact resistance and its cyclic behaviour has been evaluated. The contact resistance was found to decrease non-linearly with compression; more than 75% of reduction was attained at 2.5 MPa. The electrical contact resistance's difference between the different cycles of compression decreased with compression loads. Graphitised straight fibre Toray GDLs demonstrated the smallest contact resistance followed by the MicroPorous Layer (MPL) and the felt fibre substrate. The SGL straight fibre substrates exhibited the highest contact resistance. The felt fibre structure exhibited the smallest difference rates between the cycles of compression.

© 2020 Elsevier Ltd. All rights reserved.

1. Introduction

Although known for their high efficiency, quick start at room temperature [1], and the variety of possible applications [2] (stationary systems, mobile devices, transportation [3] and space applications [4]), the Low-Temperature Polymer Electrolyte Membrane Fuel cells - PEMFC are subject to several voltage losses

reducing their power production. Activation, Ohmic and mass transport losses are respectively predominant at low, medium and high current densities limiting the Fuel Cell - FC voltage production. Despite the continuous growth of these clean electrical generators [5] in the energy market, a larger deployment requires enhancing their reliability [6], lifespan [7–9] and reducing their costs [1]. Improving electrical power production by reducing FC voltage losses is also required. A good understanding of the influence of mechanical compression during both the stack assembly stage and the FC operation itself is necessary to reach this aim. Mechanical compression is known to reduce Ohmic losses as it decreases the resistance of the Gas Diffusion Layer - GDL and increases mass transport losses by reducing the porosity of the GDL. This is due to the high porosity of this layer making it the most sensitive element

* Corresponding author. Université Paris-Saclay, ENS Paris-Saclay, CNRS, Université Gustave Eiffel, SATIE (Systèmes et Applications des Technologies de l'Information et de l'Energie), 94235, Cachan, France.

E-mail addresses: khadidja.bouziane@utbm.fr (K. Bouziane), el-mahdi.khetabi@ifsttar.fr (E.M. Khetabi), remy.lachat@utbm.fr (R. Lachat), nada.zamel@ise.fraunhofer.de (N. Zamel), yann.meyer@utic.fr (Y. Meyer), denis.candusso@ifsttar.fr (D. Candusso).

Abbreviations		TLM	Transfer Length Method also called Transmission Line Measurement
2D/3D	Two dimensions/Three Dimensions	<i>Nomenclature</i>	
BPP	BiPolar Plate	R_c	Electrical contact resistance (Ohm)
CL	Catalyst Layer	ρ_c	Specific electrical contact resistance (mOhm.cm ²)
CCM	Catalyst Coated Membrane	W	Width of GDLs (mm)
DMA	Dynamic Mechanical Analysis machine.	L	Width of metallic indenters (mm)
GDL	Gas Diffusion Layer	d	Distance between metallic indenters (mm)
FEP	Tetrafluoroethylene-hexafluoropropylene	R_t	Total electrical resistance of the two metallic contacts and the GDL (Ohm)
FC	Fuel Cell	R_s	Sheet resistance (Ohms per square)
MEA	Membrane Electrode Assembly	A_{eff}	Specific contact area (mm ²)
MPL	MicroPorous Layer	$C_{\rho c}$	Contact resistance absolute difference between cycles (mOhm.cm ²)
PEMFC	Polymer Electrolyte Membrane Fuel Cell (also called Proton Exchange Membrane Fuel Cell)	$RC_{\rho c}$	Contact resistance relative difference between cycles (%)
PTFE	Polytetrafluoroethylene	i	cycle number
PTL	Porous Transport Layer	σ	Compression pressure (MPa)
SGL	Commercial Sigracet carbon Paper GDL series		
TGP	Commercial Toray carbon Paper GDL series		

towards compression. In this paper, the effect of cyclic mechanical compression on the electrical contact resistance between the GDL and the BiPolar Plate - BPP is analysed as this resistance is responsible of a substantial amount of Ohmic losses.

These Ohmic losses are the sum of ionic losses due to the protonic resistance of the membrane and the electronic losses caused by the bulk resistances of the other components of the cell (Gas Diffusion Layer - GDL, Bipolar Plate - BPP, Catalyst Layer - CL, Membrane) and by the contact resistances between them [10,11] (between the GDL and the CL, and between the GDL and the BPP). Contact resistances are estimated as the biggest source of electronic Ohmic losses [12,13]. They are estimated to be more than 50% of the total electronic losses [14,15] and the most significant one, between the GDL and BPP, represents 10% of the total Ohmic losses [14,15]. Because of the voltage losses, a single PEM fuel cell can produce 0.6–0.7 V, at nominal current density. In order to reach the requested power, the cells are stacked (usually up to 100 cells) electronically in series, and in parallel in terms of flows. The stack assembly is realised by a mechanical clamping system, which creates stresses [16] that affect power production.

Other external mechanical sources of stress in FC include vibrations (like in transportation system technologies) and shocks. In the other hand, FC operating conditions are responsible for internal stresses [12,13]. The swelling and shrinking of the membrane [17], depending on its water content, the difference between the thermal coefficient of the components, and to a lesser extent, the difference between reactant gas pressure induce mechanical constraints. These various internal and external loads generate an unsteady state of stress inside the FC, especially on the GDL - BPP interface. Besides, because of the nature of the BPP geometry and the GDL structure, the pressure distribution is inhomogeneous. This distribution also depends on the position of the cell inside the stack [18] and is further impacted by the nature of the clamping process. Considering the aforementioned conditions, the use of only static loads to study the effect of compression is insufficient. In addition, the structure of the GDL exhibits a nonlinear compression stress-strain curve, with a strain hysteresis along the loading-unloading cycles [19], which might become stable after 5 cycles of compression [20]. Only few studies are devoted to the impact of these cycles of compression on the physical properties of the GDL, such as electrical properties. More research needs to be conducted in order to understand their impact on the different functions of the GDL.

This porous composite media of 100–500 μm thick [21], generally made of carbon fibres either woven, carbon cloth, or non-woven, in straight and felt (spaghetti shaped) carbon fibre papers, plays different roles which require specific physical properties. First, 1) the layer must have a high porosity to provide a homogeneous reactant gas flow (H_2 in the anode and O_2 in the cathode) to the CL for an optimal use of the active surface. Besides, 2) it needs a high electrical and thermal conductivity to conduct electrons and heat to the BPP. In addition, 3) the GDL has an important role in water management; it should properly evacuate the produced water to avoid flooding and keep the pores always open to reactant gases diffusion, without drying the membrane (whose ionic conductivity is directly related to water content [11]). In this aim, GDLs are treated with a hydrophobic agent, namely PTFE or FEP [22], and sometimes, a Microporous Layer - MPL [23] is added to the GDL substrate, on the CL side. This sublayer improves the contact with the Catalyst Coated Membrane - CCM and blocks the water inside it. Researchers are developing new methods to improve water management inside the GDLs by promoting preferable water patterns [24–26], the use of porosity graded MPLs [27], the use of double gas diffusion baking layers [28,29] in self-humidified PEMFCs or by applying hydrophobic treatment on BPP [30]. Along to these functions, GDLs 4) should resist corrosion as it is in contact with different substances (BPP, water, oxygen, hydrogen). Finally, one of the most important functions of the GDL is 5) to undergo the mechanical efforts and support the MEA system so that it does not change its shape and remains functional.

As it undergoes these mechanical stresses, GDL thermal [31–33], structural [34], water management [35], durability [36], mechanical [20,37,38], and electrical properties [19,39–48] are affected, and this will influence the global cell performance. A number of papers have examined this effect [49] in order to find the optimal mechanical pressure, whereas other studies have focused on the GDL alone. M. Ahmad et al. [45] set up a numerical model that predicted a greater performance when the GDL was compressed at 1.67 MPa while N. Ul Hassan et al. [38] observed a better performance at the torque that corresponds to the most uniform pressure distribution at the BPP-GDL interface, which for the particular case of their cell was at a compression torque of 1.5 N m. T. J. Mason et al. [47] perceived the best performance at the smallest pressure of 0.5 MPa and explained that mass transport resistance was more sensitive to compression pressure as its increase with pressure was much more important

than the Ohmic resistance's decrease. This unusual observation can possibly be due to the high humidity rate of 100% of reactant gases, which enhanced water accumulation. Concluding on a particular pressure value is however difficult because of the variation of cell configurations (type of gaskets/GDLs/BPPs, assembly process ... etc) and the difference of compression approach (compression torque, GDL interfacial pressure, etc).

Other studies have focused directly on the GDL electrical properties, namely its different resistivities. It was found that the electrical conductivity of the GDL increases with compression [41] while its porosity decreases. Besides, because of the structure of the GDL, this conductivity/resistivity is anisotropic. In Ref. [50], the through-plane and in-plane conductivities of carbon paper GDLs were numerically estimated regarding the porosity rate. The through-plane conductivity was found lower than the in-plane one. Results agreed with experimentally measured conductivities with different porosity rates resulting from compression. M.S. Ismail et al. [51] also estimated the effect of GDL anisotropy by comparing isotropic/anisotropic cases. Their model shows that considering isotropic GDLs would over/underestimate the average current density (23–30%). The current density distribution was more uniform for anisotropic GDL and the in-plane anisotropy found in Ref. [52] had no significant impact on FC performance. O. Aydin et al. [43,44] measured the electrical in-plane and through-plane resistivities of paper GDLs under compression employing three different 4-point probe processes. They compared results from a gold-coated electrode method, a pin method and a micro-wire one that was deduced as the most accurate way to measure the through-plane resistivity. Both in and through-plane resistivities decreased with compression. M. Zhiani et al. [48] studied the behaviour of GDLs under compression in order to find the best MPL fabrication process. They noted a reduction of electrical in-plane resistivity and gas permeability with compression. They selected the ultra-sonic bath as the best MPL fabrication process compared to pulse sonication, continuous sonication, and mechanical stirring ultra-sonic as it provided a good trade-off between a low resistivity and an acceptable permeability. M. Hamour et al. [46] found that the in-plane conductivity of cloth GDLs increased by 45% at a 4 MPa compression and reached 50% at 8 MPa.

Despite the number of papers on the bulk resistivity of the GDL, most studies have been done under static compression, except for the work of D. Todd [53] and Qui D [54], where cyclic compression was used.

D. Todd et al. [53] measured the through-plane resistivity and both fibre and cross fibre alignment direction in-plane resistivities of a carbon paper GDL under cyclic compression. They noticed a decrease of all resistivities with compression, with the lowest in-plane resistivity measured in the direction of fibre alignment. They also observed a decrease in the through-plane resistivity during cycling, while the in-plane resistivity increased. In Ref. [54], the electrical resistance of the 3 different structures (carbon cloth and straight/felt fibre papers) of GDL has been investigated under cyclic mechanical compression, and the through-plane resistance has been extracted using GDLs with different thicknesses. They found that felt structure was the most stable one.

Regarding the electrical contact resistance between the GDL and the BPP, focus was also given to static compression. This electrical contact resistance was found to decrease with compression [19,39,40], [55–57]. Three main methods were used to determine the contact resistance. A subtraction method [56,57] can be used by measuring the electrical resistance of two assemblies in such a way that the difference between the assemblies' resistances gives the desired contact resistance. However, most studies that used this method neglected either the bulk resistance or its variation with compression. Another constraint is the difficulty of using this

method with GDLs having non-identical sides such as one side MPL coated GDLs. The contact resistance can also be determined by a numerical or experimental estimation that can be achieved using results of the subtraction method. For instance, in Ref. [55], T. J. Mason et al. estimated this contact resistance, by placing a GDL between 2 compressed BPPs and by measuring the resistance under compression, the entire resistance was attributed to the contact resistance. An estimation process can also be used to determine the variation of the through-plane resistance of the GDL with compression, from its porosity such as in the work of M.S. Ismail et al. [40]. They concluded that compression reduces the contact resistance and that it is influenced by the GDL's initial thickness in the presence of a gasket. They also denoted a better contact when the MPL is more loaded with PTFE. A numerical model can also be set to obtain the global contact resistance using experimental results with a flat graphite plate [58–60].

Finally, the use of the Transmission Line Method - TLM allows a direct experimental determination of the contact resistance of each side of the GDL. D. Ye et al. [15] employed a TLM method to measure the contact resistance under static compression and concluded no dependence on clamping pressure. S. El Oualid et al. [19] set up a TLM method to measure the contact resistance, that was found to decrease with compression non-linearly.

Despite the numerous ways of determination of contact resistance under compression, just as in the case of bulk resistivity, most studies have been done under static compression, even if GDL have been preconditioned in some studies ([19,55,57].) Neither the real quantification of the effect of cyclic compression on the contact resistance of GDLs, nor the effect of structural parameters is available in literature. Only one study has used cyclic compression [55] when measuring contact resistance: they found a dependence of this resistance to the cycles of compression. However, the total resistance was estimated as the contact resistance. The relationship between the different structures and composition of GDL and the effect of the cycles of compression on the contact resistance is still not explored and to the knowledge of the authors, no study has determined the effect of cyclic compression on the electrical contact resistance measured by the TLM method.

In this paper, we determine the electrical contact resistance between the GDL and the BPP, using a TLM method under cyclic mechanical compression from 0 to 8 MPa. A quantification of the effect of the cycles of compression is given. In addition, the effect of PTFE, MPL, and different carbon paper GDL structures is analysed. In the next section, a brief explanation of the experimental method and data analysis is given. In the third section, mechanical aspects are treated followed by the analysis of the electrical contact resistance behaviour towards mechanical compression, the effect of structure and composition and the influence of cyclic compression on mechanical and electrical parameters. Before concluding this paper, the results are compared to the literature.

2. Experimental procedure

The electrical contact resistance (R_c) (and its specific value ρ_c) between the GDL and the BPP were evaluated under cyclic mechanical compression using an ex-situ testing method similar to the study of S. El Oualid et al. [19]. However, we employed a mechanical force and a contact area different from Ref. [19], and considered six types of GDL samples. The measurement of the contact resistance was carried out according to the Transmission Line Method (TLM); a brief explanation of the method is given in Section 2.3.

2.1. Samples and sample holder

Six different types of carbon paper GDL samples were used (Cf.

Table 1). The SGL 24 BC is coated with a MPL at one side. Even though the MPL usually faces the CL, both the fibres substrate side and the MPL one were evaluated.

The samples were cut into two sheets, each with a width ($W/2$) of 2 mm and a length of 40 mm (Fig. 1 a). They were disposed at each side of the sample holder in order to guarantee some mechanical stability. This homemade sample holder was specifically designed to ensure the application of a homogenous mechanical compression on the samples, thanks to its ball device. The sample holder includes two gold coated metallic indenters with a width L of 1 mm, which is a typical size of BPP rib width. These indenters are in contact with the GDL samples on 4 contact surfaces of $W/2 \times L = 2 \times 1 \text{ mm}^2$ areas each, making a total contact area of 8 mm^2 .

The GDL-indenter system is electrically insulated from the machine with two glass plates. The upper plate is designed in a way that allows the variation of the distance between the indenters d ($d1$ to $d4$) (Table 2), which is required to evaluate the contact resistance R_c using the TLM method (Fig. 1 b). This method is based on the fact that the total resistance R_t (between two metallic contacts and the GDL) is proportional to the distance between the two metallic contacts d .

2.2. The mechanical load

A cyclic mechanical compression has been applied on the GDL samples using a Dynamic Mechanical Analysis machine - DMA type Metravib VA2000. GDLs were compressed by the indenters, i.e. the 4 compressed surfaces, which are the 4 contact surfaces forming a total compressed area of 8 mm^2 . The mechanical force ranged from 0 to 65 N ($\pm 0.2 \text{ N}$); in terms of applied stress: 0–8.25 MPa ($\pm 0.025 \text{ MPa}$). Five cycles of loading-unloading compression were applied with four levels of pressure as shown in Fig. 2. This cyclic loading has been applied three consecutive times for every distance d (i.e. $d1, d2, d3, d4$), on each GDL sample.

2.3. Specific electrical contact resistance determination

As mentioned earlier, the electrical contact resistance measurement method applied in this research is the TLM method, which is usually used to measure the electrical contact resistance between a metal and a semi-conductor. This method is based on the fact that the total resistance between two metallic contacts and the GDL (R_t) is proportional to the distance between the two metallic contacts (d) following Eq. (1):

$$R_t = R_s \frac{d}{W} + 2R_c = a \cdot (d) + b \quad (1)$$

with:

- R_s : the sheet resistance (Ohms per square).
- W : the width of the GDLs (mm).
- R_c : the contact resistance (Ohm).
- d : the distance between the metallic indenters (mm).

Table 1
GDL sample type.

GDL type	Thickness (μm)	Structure and composition
SGL 24 AA	190 ± 30^a	Straight carbon fibre paper.
SGL 24 BA	190 ± 30^a	Straight carbon fibre paper with 5% PTFE (hydrophobic agent).
SGL 24 BC	235 ± 30^a	Straight carbon fibre paper with 5% PTFE + MPL.
Toray TGP H90	280 [61]	Graphitised straight carbon fibre paper.
Toray TGP H120	370 [61]	Graphitised straight carbon fibre paper.
Freudenberg H2315 I3	210 [62]	Felt Carbon fibre paper + hydrophobic agent.

^a From SGL carbon company.

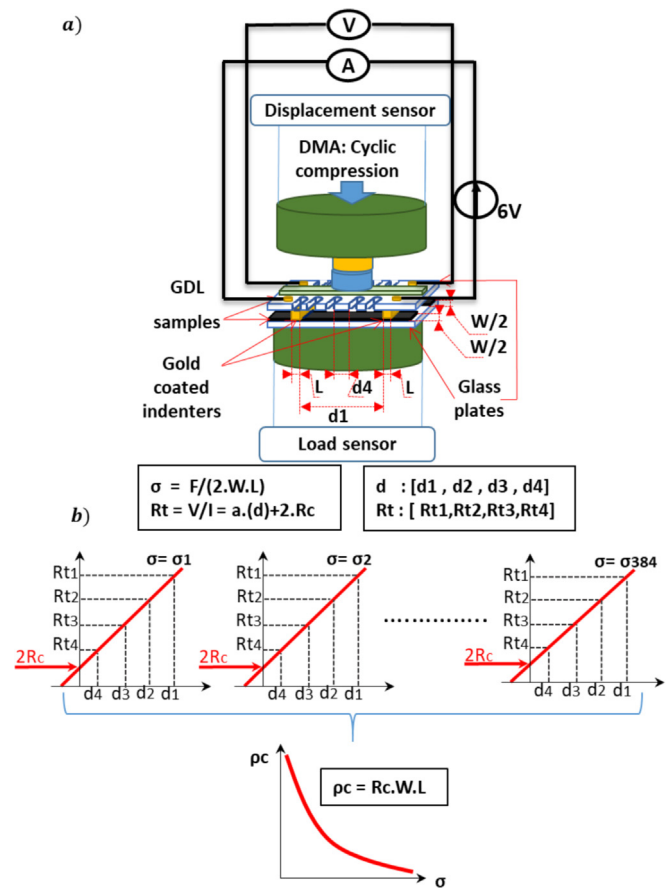


Fig. 1. Graphic summarising the experimental procedure to estimate the electrical contact resistance between the GDL and the BPP under cyclic mechanical compression. a) Experimental set-up, b) Contact resistance (R_c) extraction.

Table 2
Distances between the two indenters.

Distance name	Length (mm) ($\pm 5\%$)
$d1$	31.1
$d2$	18.1
$d3$	9.9
$d4$	2.2

The contact resistance R_c can be determined by varying the distance between the metallic indenters d in order to find the slope a and the offset b of the linear curve $R_t = f(d)$. In this study, four values of d have been used as shown in Table 2.

The slope $a = R_s/W$ and the offset $b = 2 \cdot R_c$ are then extracted using the least square method. The specific electrical contact resistance is obtained by multiplying the contact resistance by the specific area of one side of the contacts (A_{eff}):

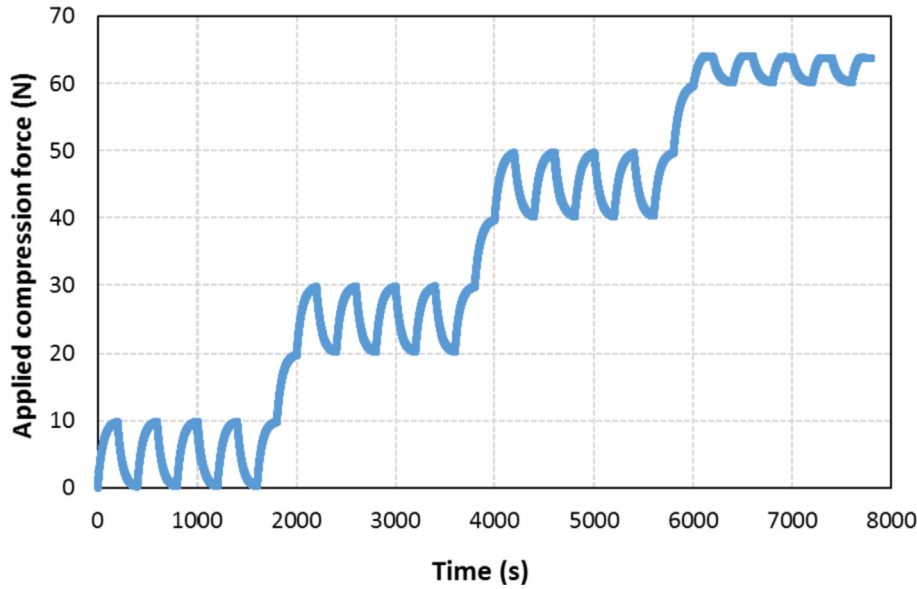


Fig. 2. Applied mechanical load.

$$\rho c = R_c \cdot A_{eff} \quad (2)$$

So that:

$$\rho c = R_c \cdot W \cdot L \quad (3)$$

with: $W \cdot L = 4 \text{ mm}^2$.

For more details on the mathematical model of the TLM method, the reader is referred to Refs. [63–68]. The electric circuit composition is similar to the circuit of [19]. The GDL-indenters set is included in an electrical circuit with a fixed voltage source and a witness resistance. Voltage and current are measured across the system and the total resistance R_t is evaluated as a function of compression for every distance d . The voltage generator is set to 6 V. (Fig. 1 a), as El Oualid S. et al. [19] has found that this value was more suitable for a linear relation between (R_t) and (d). The voltage and the current resolutions are 2 mV and 0.1 mA, respectively. Uncertainties were determined using the evaluation of type B [69]; which is a way to evaluate uncertainties using non-statistical methods (such as the use of previous data measurement, manufacturer specification, calibration reports ... etc), in our case, the manufacturer' specifications were used. Uncertainties on the measured voltage U and current I , were determined according to the user manual of the Oscilloscope used (Tektronix tds2002) with an accuracy of 3% on the measured values. Uncertainty on R_t was calculated according to error propagation laws applied to U and I . Uncertainty on R_c was extracted from the uncertainty on the offset (b) calculated according to the ordinary least-square method, by considering the highest uncertainty on R_t and neglecting the uncertainty on d .

2.4. The data analysis process

Experimental data were collected by an acquisition card. The same experimental process was followed for the seven sample types (including the MPL side of SGL 24 BC). First, the distance between indenters d was fixed, starting by the longest distance d_1 , so that the material between the indenters is always uncompressed and not damaged by previous compression. Then, an electromechanical test was done through applying a voltage of 6V to the

circuit (Fig. 1) under the mechanical load depicted in Fig. 2. The total resistance between the indenters R_t is measured, as well as the displacement of the GDL. The data was stored in one file corresponding to d_1 . Then, the same test was repeated twice again on the same sample and the data was stored in the same spreadsheet file (tests 1, 2 and 3). The same process was repeated for the three other distances d and the data was recorded in three other files. The four files obtained are treated in order to obtain the contact resistance R_c and the total strain as a function of the applied stress. Every file consists of a number of data sequences. Each data sequence includes: measured force, target force, measured displacement, current intensity, voltage, and time. The number of data sequences in each file is reduced to 384 measurement points by using a simple moving average of the current intensity, the voltage and the displacement by step of 1N of measured force.

For every GDL, the four files of the measured resistances R_t for the four distances d are combined to calculate the contact resistance using the least square method and the average strain. E.g. the measurement point 5 corresponds to a loading compression of 0.5 MPa for the first cycle of compression, the contact resistance for this point of pressure is calculated using the 4 total resistances R_t (for d_1, d_2, d_3, d_4) at this point of compression using the least square method according to Eq. (1). The steps of the experimental process are depicted in Fig. 1.

Fig. 3 shows the relationship between R_t and d , for the SGL 24 AA. We can observe that the experimental points are quite linear with a regression coefficient of 96%. Accurate measurement of R_c involves a good alignment of the points formed by $R_t=f(d)$ which requires a high regression coefficient.

3. Results and discussion

The following section describes the mechanical and the electrical behaviour of the GDLs under cyclic mechanical compression, followed by a detailed discussion on the difference of electrical and mechanical parameters obtained by this cyclic compression.

3.1. The mechanical behaviour of the GDLs

For every GDL, the total strain was determined by calculating an

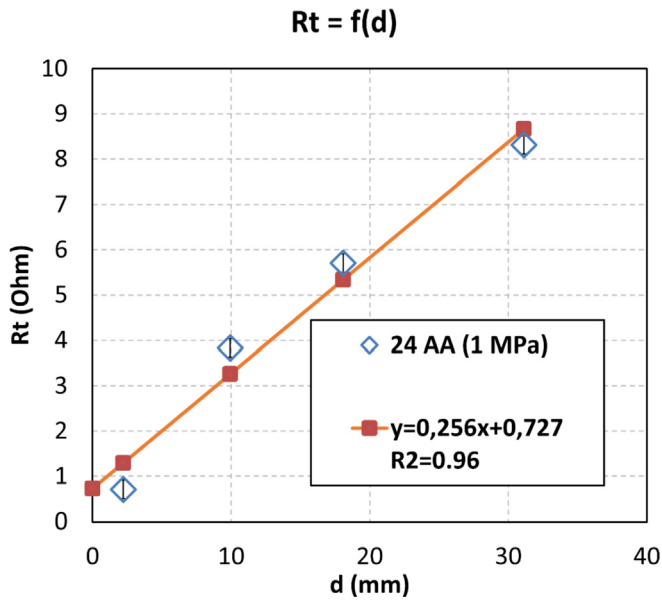


Fig. 3. Real $R_t = f(d)$ and least square line for SGL 24 AA, first test.

average of the total displacements measured (d_1 , d_2 , d_3 or d_4). The average value is then divided by the initial thickness given in the material datasheet (Cf. Table 1).

One source of uncertainty is the unstable initial position of the sample holder, as well as the inaccurate GDL initial thickness value due to the material structure of the GDL that is similar to a fabric-structure. These two issues are the cause of displacement starting point related uncertainties. To limit these uncertainties, the initial position has always been set less than ($\pm 10 \mu\text{m}$) in terms of displacement with an initial force less than ($\pm 0.2\text{N}$).

When comparing the thickness of Toray samples and the SGL 24 BC samples of this investigation with the study of A. El-Kharouf et al. [70] at the compression pressures of 0.5 and 2.5 MPa, less than 12% difference was observed for the Toray and less than 24% for the SGL. This difference can be explained by the use of another type of compression load and other experimental variations.

Fig. 4 shows the mechanical stress-strain of every GDL for the first test. Three main levels of stiffness are observed for all GDLs. A stiffer group composed of the Freudenberg GDL and the MPL side of the SGL 24 BC, a medium group including the remaining GDLs apart from the SGL 24 AA, which composes alone the soft level and last group. For the Sigracet series, we can first notice that the SGL 24 BA is much stiffer than the SGL 24 AA, as well as the SGL 24 BC. Two different stress-strain curves were obtained when compressing the SGL 24 BC from each side (the MPL side and the substrate one). For the Toray series, the samples belong to the medium level and the Toray H90 exhibits a stiffer behaviour.

3.1.1. Effect of PTFE

The higher stiffness of the SGL 24 BA compared to the SGL 24 AA is the result of the 5 wt% of PTFE added to the 24 BA, which is the only distinction of composition between the two GDLs. The PTFE covers the carbon fibres and mechanically locks their movement making the substrate stiffer.

3.1.2. Effect of the MPL

The SGL 24 BC is originally a substrate of type SGL 24 BA covered with a MPL at one side. When compressing this SGL 24 BC from two different sides (the substrate side or Porous Transport Layer side - PTL and the MPL side), two different curves were obtained. We

expect that the result of the deformation curves represents mainly the deformation of the upper compressed layer, along with a slight compression of the lower layer. It is noteworthy to mention that for the first loading cycle of compression from 0 to 0.7 MPa the two curves are quite similar.

3.1.3. Effect of structure and fabrication process

The materials from Toray have comparable mechanical stiffness curves with the SGL 24 BC PTL side and the SGL 24 BA, which are hydrophobic straight carbon fibre papers. The felt carbon paper of Freudenberg is stiffer compared to the straight carbon fibre structures. It has the same mechanical behaviour as the MPL side of the 24 BC.

3.2. The specific electrical contact resistance

As expected, the experiments described a non-linear decrease of the specific electrical contact resistance ρ_c with compression as shown in Fig. 5. A very rapid reduction of ρ_c from 0 to 3 MPa can be observed, then a slower one from 3 to 8 MPa. For all the GDLs, more than 75% of the total reduction of ρ_c is obtained at 2.5 MPa. The applied stress improves the contact between the GDL and the indenters by increasing the contact surface. It also decreases the porosity of the GDL, making carbon fibres that conduct electrons closer to each other.

At first glance, the Toray GDLs manifested a small specific electrical contact resistance ρ_c (4–20 $\text{m}\Omega\cdot\text{cm}^2$), SGL GDLs a higher one (4–65 $\text{m}\Omega\cdot\text{cm}^2$), while the Freudenberg had a medium contact resistance (8–32 $\text{m}\Omega\cdot\text{cm}^2$) (Fig. 5 a)). In the SGL group, the PTL side of the 24 BC shows the highest resistance (27–65 $\text{m}\Omega\cdot\text{cm}^2$) while its MPL side displays the lowest one (4–23 $\text{m}\Omega\cdot\text{cm}^2$). The SGL 24 BA has a higher resistance compared to the SGL 24 AA as shown in Fig. 5 b). For the Toray Series, the Toray H120 has a comparable resistance with the H90. Some scattered points can be observed when pressure is lower than 1.25 MPa, even after 2 previous tests reaching 8 MPa as depicted in Fig. 5.

Uncertainties on ρ_c are reported in Fig. 5 b); they will be discussed in Section 3.2.3.

3.2.1. Effect of PTFE loading

Analogously to the mechanical behaviour, the fact that the SGL 24 BA has a higher electrical contact resistance compared to the SGL 24 AA is ascribed to the PTFE which is added to the reference 24 BA (5 wt%). The PTFE is a non-conductive material that can cover some of the contact surfaces with the indenters. However, more importantly, it increases the mechanical resistance limiting the compression rate of the GDL, which will limit the decrease of the contact resistance attributed to the larger contact area enhanced by compression. This can explain the visible increase of the gap between the resistance of the 24 AA and the 24 BA with compression (from 0 to 1 MPa) that is observed in Fig. 5 a).

3.2.2. Effect of the MPL

With its smooth surface, the MPL of the SGL 24 BC improves the contact with the indenters, which decreases the contact resistance of the MPL side. The SGL 24 BC PTL side, which originally has the same structure and composition of the SGL 24 BA, exhibited a higher contact resistance compared to the SGL 24 BA's one. Because the contact resistance measured also includes the contact resistance between the MPL and PTL side of the GDL that should also be taken into consideration when analysing Ohmic resistances. We expect that the measurement of R_c at the PTL side of 24 BC contains also the contact resistance between the PTL and the MPL interface. This is not the case when ρ_c is measured at the MPL side because

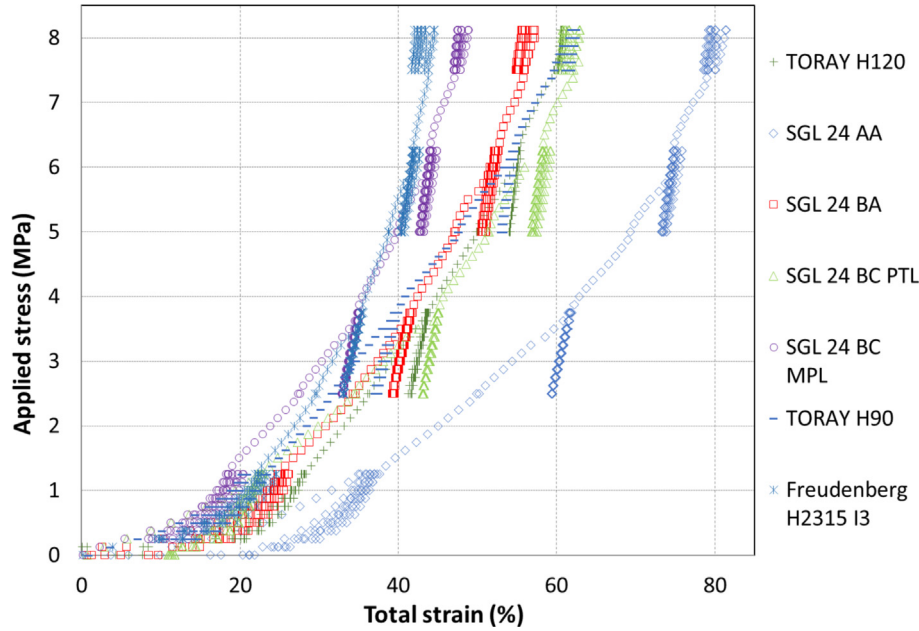


Fig. 4. Stress-strain curves.

the MPL bulk resistance might be much lower than the MPL substrate contact resistance and the PTL bulk resistance. Therefore, the current flows only from the first indenter through the MPL layer, then get back to the second indenter without passing through the lower layer (PTL side, i.e. macroporous layer side), in the case of the MPL side measurement.

3.2.3. Effect of structure and composition

The felt carbon paper exhibited a resistance value between those of SGL straight carbon paper 24 AA and 24 BA. The smallest resistances were measured for the graphitised straight carbon papers of Toray. Graphitised and felt structure are also showing smaller uncertainty values compared to the straight paper GDLs as shown in Table 3.

3.3. Effect of the cycles of compression

3.3.1. Effect on the contact resistance ρ_c

While measuring the electrical contact resistance, the GDLs were compressed from 0 to 8.25 MPa. They were subjected to 5 cycles of loading-unloading mechanical compression upon four levels of compression (0–1.25 MPa, 2.5–3.75 MPa, 5–6.25 MPa, and 7.5–8.25 MPa) (Fig. 2).

The effect of the cycles of compression has been evaluated with two methods by calculating an absolute value and a relative one. The absolute difference of contact resistance ρ_c between the cycles $C\rho_c$ has been evaluated by determining the average of the absolute value of the difference between ρ_c at the loading of the 2nd, 3rd, 4th, and 5th cycle and ρ_c at the loading of the 1st cycle (Cf. Eq (4)). The rate of this difference $RC\rho_c$ was extracted by dividing it by the value of ρ_c at the 1st cycle (Cf. Eq (5)). The effect of the cyclic compression on the mechanical properties has been evaluated in the same way, using the strain instead of ρ_c . One pressure value has been chosen for every compression level: 1, 3, 6, and 8 MPa. Standard deviation has been evaluated for absolute values.

$$C\rho_c = \frac{\sum_{i=1}^5 (\rho_{c1} - \rho_{ci})}{4} \quad (4)$$

$$RC\rho_c = \frac{C\rho_c}{\rho_{c1}} \times 100\% \quad (5)$$

with:

$C\rho_c$: Contact resistance absolute difference between cycles (mOhm.cm²).

$RC\rho_c$: Contact resistance relative difference between cycles (%).

ρ_{ci} : Specific electrical contact resistance at cycle i (mOhm.cm²).

The electrical contact resistance is globally affected by the number of cycles of compression. As expected, we observe a general trend of decrease of the difference between cycles ($C\rho_c$ and $RC\rho_c$) with compression for all GDLs, as well as the difference for strain values. The difference between cycles for compression values of 1 and 3 MPa is much higher than for values of 6 and 8 MPa (Fig. 6). This decrease is higher in absolute values $C\rho_c$ and less evident in relative values $RC\rho_c$ because the contact resistance itself decreases with compression (Fig. 6). Values of $C\rho_c$ depicted a maximum mean value of 8.9 mOhm.cm² for the SGL 24 BC substrate sample.

When analysing the absolute values (Fig. 6), the Toray H120 manifested a low difference between cycles followed by the Freudenberg H2315 I3, while the highest ones were presented by the GDL 24 BC substrate side (PTL) followed by its MPL side. We can imagine that the Toray graphitised structure is the least sensitive to the mechanical cyclic issues. Yet, when observing the relative values, this H120 had to some degree higher difference rates. This is explained by the fact that its contact resistance is so low compared to other GDLs that even values of less than 1.2 mOhm.cm² give relative differences $RC\rho_c$ of about 48%. The Freudenberg, on the other hand, had the lowest difference rate $RC\rho_c$ (Fig. 6 a) and b)), which is attributed to its 3D felt structure being less sensitive to cyclic effects compared to the 2D straight carbon fibre structures. Observing the mechanical properties regarding the difference between cycles, it is visible that, for absolute and relative difference of strain, the Freudenberg H2315 I3 had the lowest value as well (Fig. 7), which confirms that its structure is the least sensitive to cyclic compression and therefore its ρ_c as well. Qiu D. et al. [54] also concluded that the felt carbon structure had the highest stability in terms of electrical resistance and microstructure after applying

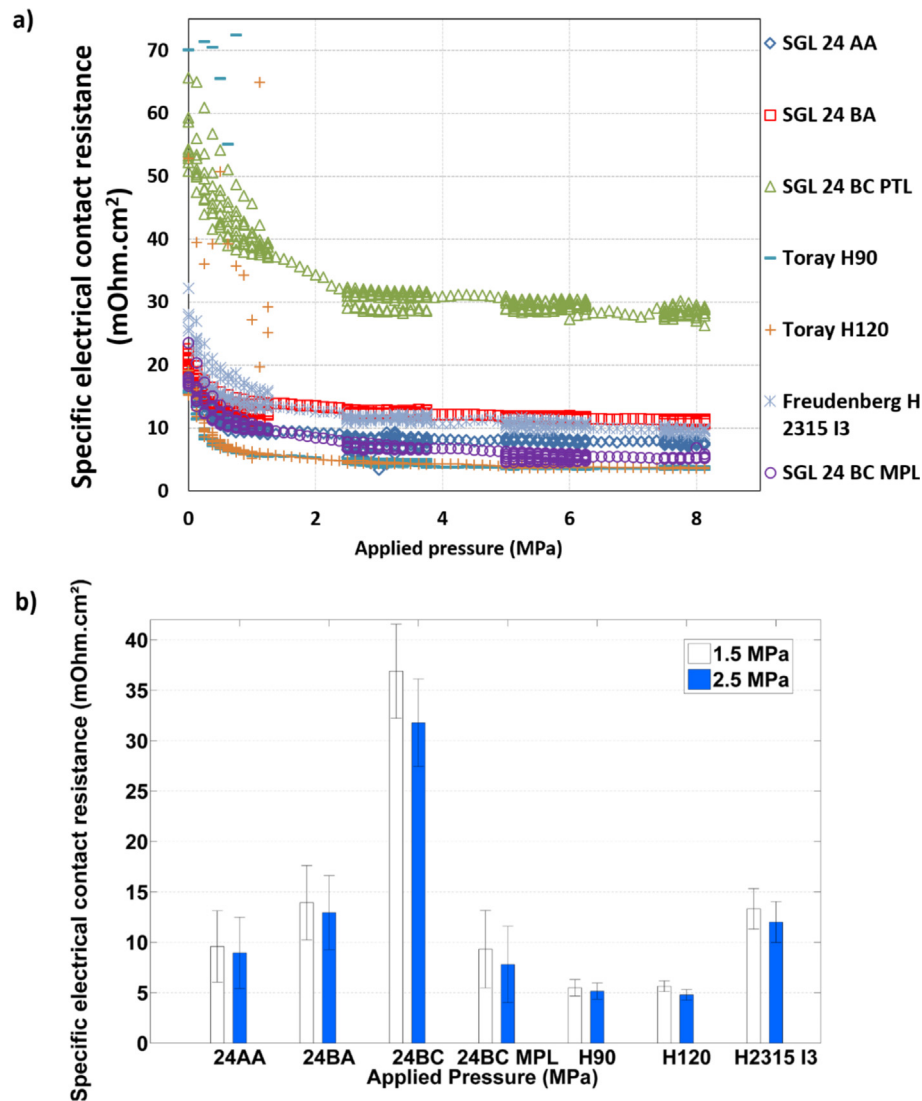


Fig. 5. a) Electrical contact resistance as a function of the applied stress for the third test. b) Electrical contact resistance with uncertainties at 1.5 and 2.5 MPa.

Table 3

Uncertainties of the contact resistance (3rd test).

GDL		24 AA	24 BA	24 BC	24 BC MPL	H90	H120	H2315 I3
Uncertainty on ρ_c (mOhm.cm ²)	Minimum	3,52	3,61	4,18	3,56	0,71	0,51	1,97
	Maximum	3,68	3,92	4,99	4,33	1,23	0,74	2,25
	Average	3,54	3,68	4,54	3,79	0,81	0,53	2,05
Average relative uncertainty (%)		41,89	29,62	13,84	55,52	18,16	11,47	17,29

cyclic and steady loads. We also notice that the 24 BC GDL is mechanically the most sensitive GDL to strain difference between cycles just as it is in terms of $C_{\rho c}$.

3.3.2. Effect of PTFE

The difference between cycles $C_{\rho c}$ of the 24 BA increased unexpectedly compared to the 24 AA. It appears that the PTFE increases the electrical sensitivity to cyclic compression. This is not explained by the mechanical difference between cycles, which decreased with PTFE. The increase of the $C_{\rho c}$ may be attributed to the PTFE deterioration with cycles.

3.3.3. Effect of MPL loading

The 24 BC GDL substrate, which has originally the same structure as the 24 BA, exhibited a higher absolute and relative difference $C_{\rho c}$ and $RC_{\rho c}$. The MPL side of the 24 BC also showed a higher $RC_{\rho c}$ at low pressure. Adding a MPL increased the difference between cycles of the GDL substrate side, electrically and mechanically.

3.3.4. Effect of the three tests of mechanical compression

The mean electrical contact resistance is almost constant over the three consecutive compression tests for all the GDL types with a trend of a slight decrease of ρ_c along the tests for the SGL GDLs

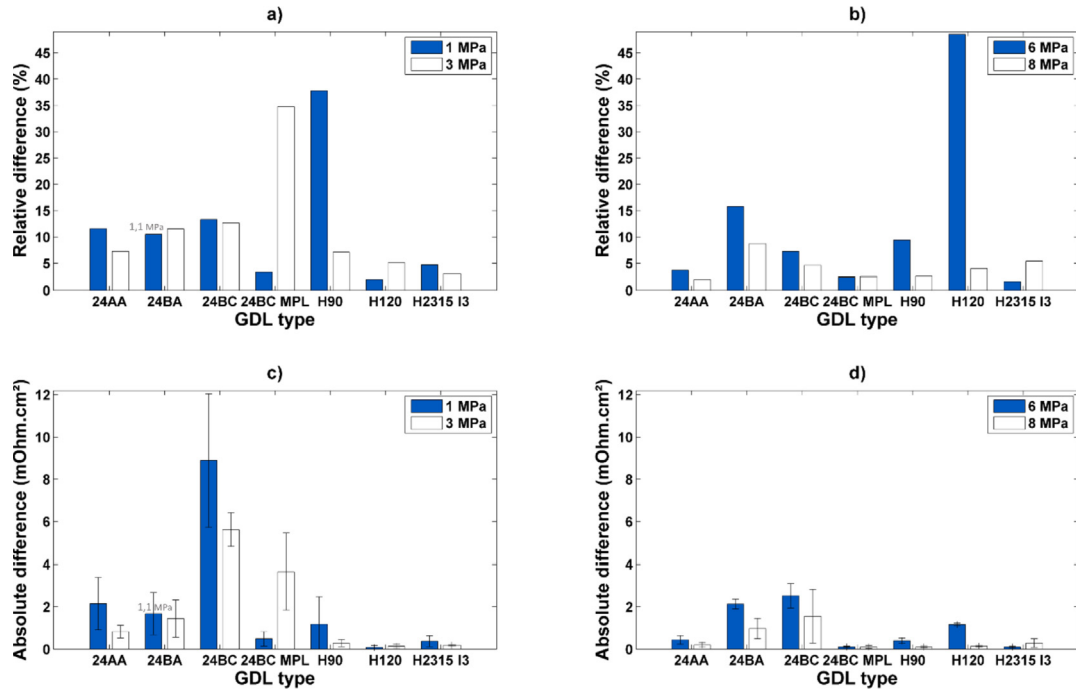


Fig. 6. The difference of Contact resistance between cycles as a function of compression pressure: the relative difference $RC_{\rho c}$ at low pressure and b) at high pressure. The absolute difference $C_{\rho c}$ c) at low pressure and d) at high pressure.

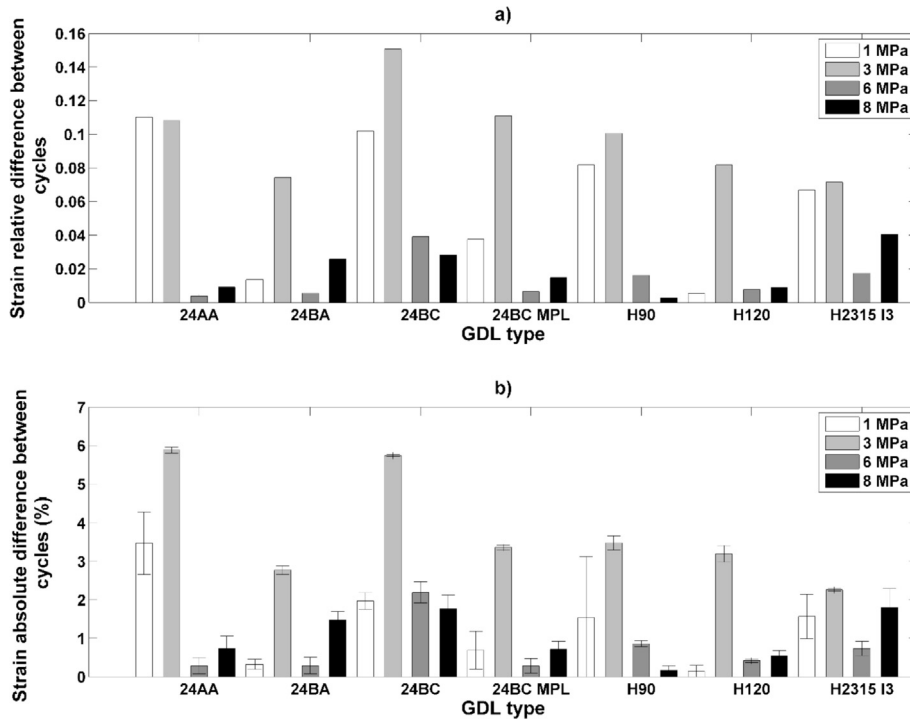


Fig. 7. Strain difference between cycles for 1, 3, 6 and 8 MPa, with standard deviations.

(Fig. 8) and a little increase of ρc for the other GDLs. The $C_{\rho c}$ tends generally to diminish with the tests.

3.3.5. Effect of cyclic compression on the FC efficiency

For a cell with an Ohmic resistance of 150 mOhm.cm², and a compression pressure of 1 MPa applied on a GDL, the variation of

the BPP-GDL contact resistance due to the cycles of compression depending on the GDL type ranges from 1 to 8 mOhm.cm², and will contribute by 1.3–10.6% to the total Ohmic losses. For a cell of 200 cm² at a current of 1 A/cm² and a cell voltage of 0.5V, this will impact the produced power by 0.4–3.2 W (i.e. about 0.4%–3.2% of the total electrical power produced by the cell). This amount (of the

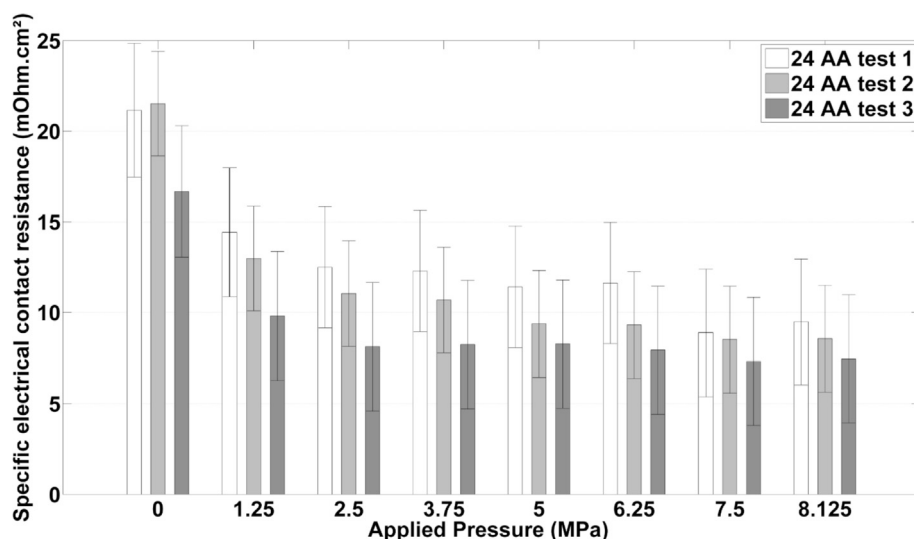


Fig. 8. Electrical contact resistance as a function of the applied stress for the three tests performed with SGL 24 AA.

energy delivered by the cell) can be considered as significant in the context of a widespread deployment of FC technologies and regarding the total energy losses of the FC generator fleet.

3.4. Comparison with literature values

Table 4 is a summary of some results found in literature, from studies that considered the same GDLs and measured the electrical contact resistance between the GDL and the BPP under mechanical compression. Most values are selected for compression stresses of 1.5 MPa and 2.5 MPa in order to compare between different studies.

In these works, different methods of measurement are used. The electrical contact resistance are measured by the TLM method [15,19], (and this study), a subtraction method [56,57] or estimated [55]. In some studies, the GDLs are pre-conditioned or cyclic compression is applied [19,55,57], (and this study). BPPs or gold covered electrodes are employed [19,56,57], (and this study).

We compared the contact resistance measured in the first cycle of the third test for the GDLs used in this study, in order to take into account the previous cyclic compression. For the Toray H120, the contact resistance decreased in this study from 5.6 mOhm.cm² at 1.5 MPa to 4.8 mOhm.cm² at 2.5 MPa (Table 4). T. J. Mason et al. [55] estimated that it decreases from 14 mOhm.cm² to 9.9 mOhm.cm²; this difference can be attributed to the fact that their measurement value included the bulk resistance of the GDL and because of the use of a 5% PTFE treated H120 sample. In addition, BPPs were not gold coated. In a subtraction method used by A. El-kharouf [57], this resistance was found equal to 4.6 mOhm.cm² at 1.5 MPa and decreased to 3.23 mOhm.cm² at 2.5 MPa. D. Ye et al. [15] found a resistance of 12–13 mOhm.cm² that did not change much with compression; they used a TLM method with copper indenters and a Toray H120 with 20 wt% of PTFE. This higher resistance can be due to the copper electrodes and because of the presence of PTFE. This may also be the reason why there was no notable change with compression as the PTFE is known to increase the stiffness of GDLs.

According to the different studies that employed the Toray H90, the contact resistance at these pressure levels is in the range of 1–10 mOhm.cm², with the common characteristics of decreasing with compression. However, when A. Miyazawa et al. [56] used no gold coating, it ranged from 50 to 100 mOhm.cm².

The SGL24 BA's contact resistance ranges from 2 to 35 mOhm.cm².

It is then clear that the contact resistance measured is dependent on the measurement apparatus and specifically on the electrode used. However, almost all studies found that the contact resistance decreases with compression. Methods with gold coating gave relatively lower electrical resistance values compared to those with bare stainless steel or copper surfaces and the subtraction method gave a lower contact resistance compared to the TLM.

4. Conclusion

In order to study the effect of the variability of the mechanical stress exerted on a GDL inside a PEMFC, a cyclic mechanical compression was applied on a variety of carbon paper GDLs while measuring their specific electrical contact resistance with the BPP using the TLM method. The influence of the GDL structure and composition was analysed. The experiments describe a non-linear decrease of the electrical contact resistance with compression, a very rapid reduction from 0 to 3 MPa, then a slower one from 3 to 8 MPa. A pressure of 2.5 MPa exerted on GDLs should be sufficient to insure an acceptable range of contact resistance inside a PEMFC. Besides, this contact resistance is affected by the cycles of compression. The difference between cycles of the contact resistance and the strain tends, however, to decrease with higher compression values. Furthermore, it is notable that the mean electrical contact resistance is almost constant over the three consecutive mechanical tests for all GDLs and that generally, the electrical difference between cycles tends to decrease along the tests.

Regarding the impact of composition and structure, in terms of electrical contact resistance, graphitised GDLs displayed the smallest contact resistance followed by MPL covered GDLs (MPL side) then felt and straight fibre paper GDLs. In terms of stiffness, the felt carbon structure and the MPL side of the SGL 24 BC, exhibited, again closely, the highest rigidity. Besides, it is noteworthy that the PTFE increased the mechanical stiffness of the GDL, increasing with that the contact resistance. Finally, PTFE treated GDLs and graphitised structures were stiffer than the simple untreated GDLs. In terms of the difference between the cycles of compression, the felt GDL structure was denoted as the least sensitive to cyclic compression and the double layer GDL 24 BC as the most affected. The mechanical difference between cycles explains a substantial part of the electrical one, such as the felt structure and the double layer's behaviours but it is still not sufficient to explain

Table 4

The electrical contact resistance measured with different methods described in the literature and in this study.

GDL studied	Compression pressure Vs ρ_c		Method of measurement or estimation (in literature)	Ref.
	σ (MPa)	ρ_c (mOhm.cm ²)		
Toray H120 (5 wt% PTFE)	1.4	1st: 15 (loading)/12 (unloading) 7th: 17	A GDL was put between two BPPs (graphite) and the set was compressed (CCU). Then, the resistance between the two BPPs was measured. The measured value was considered as the contact resistance because of the small values of the GDL and BPP bulk resistances. The effect of the numbers of cycles of compression was studied by unloading back to 0.2 MPa for every pressure value (from 0.2 to 2.5 MPa) (14 cycles). The active area: 6.2 cm ² . The rib area (compressed area): 3.3 cm ² .	[55] (Average value + cyclic compression)
	1.6	1st: 13 (loading)/10 (unloading) 8th: 18		
	1.5: mean	1st: 14 (loading)/11 (unloading) 8th: 17.5		
	2.5	1st: 9.9 14th: 13.5		
	1.4	1st: 11.7		
SGL 24 BA	1.6	1st: 10.6		
	1.5: mean	1st: 11.2		
	2.5	1st: 7.9		
	1.4	0.9: Au and Ni coating		
	1.6	0.8: Au and Ni coating		
Toray H90	1.5: mean	0.85: Au and Ni coating	1. A GDL was put between 2 compressed copper electrodes and the resistance R_{GDL} was measured. 2. A BPP (stainless steel SS316L) was put between 2 GDLs that were between 2 compressed copper electrodes and the resistance R_{all} was measured. 3. The specific electrical contact resistance between the GDL and BPP was calculated: $R_{cr} = S1 (R_{all} - 2R_{gdl})/2$ The BPPs were covered by gold with different thicknesses; in some samples an intermediate layer of 100 nm of Ni was added before gold coating. No GDL compression preconditioning has been done. The active electrode area: 3.14 cm ² (electrode diameter: d = 2 cm).	[56] (Subtraction method + gold coating)
	2.4	1.7: Au coating		
	2.6	0.76: Au and Ni coating		
	2.5: mean	0.70: Au and Ni coating		
	2.5	0.73: Au and Ni coating		
	1.5	1.4: Au coating		
	2.5	100 (without any coating)		
	4	50 (without any coating)		
		44 (without any coating)		
Toray H120 (+PTFE)	1.5	4.60	1. A GDL was put between 2 compressed graphite BPPs which were placed between 2 stainless steel gold covered electrodes and the resistance $R_{measured}$ was measured.	[57] (subtraction + gold coated electrodes + pre-conditioning of GDLs)
	2.5	3.23		
Toray H90 (+PTFE)	1.5	3.64	2. A BPP was put between the 2 compressed stainless steel gold covered electrodes and the resistance $R_{BPP, measured}$ was measured.	
	2.5	2.77		
SGL 24 BA	1.5	2.69	3. The GDL and BPP through plane resistances were neglected and the contact resistance between the GDL and the BPP was calculated as: $R_c = (R_{measured} - R_{BPP, measured})/2$. The GDLs were preconditioned by applying a 3 MPa pressure 3 times. The area of samples: 4 cm ² .	
	2.5	1.76		
Toray H120 (20 wt% PTFE)	0.8	12.8	- The TLM method was used to find the contact resistance by measuring the voltage between several copper pads with different distances. - The inhomogeneous compression was modelled by using different sizes of channels/ribs and blocks. - Compression pressure (deduced from GDL thickness): 0.27 MPa–2.16 MPa.	[15] (TLM + Copper indenters)
	0.27	13 (no much difference)		
	–2.16			
SGL 24 AA	1.5	28	- The TLM method was used to measure the electrical contact resistance of GDLs. - Gold-coated indenters were employed.	[19] (TLM + Gold covered indenters + Pre-conditioning of GDLs)
	2.5	25		
SGL 24 BA	1.5	32.5	- A Dynamic Mechanical Analysis machine-DMA was used to apply a mechanical excitation (static compression force of (–10 to –60 N) on a surface of 6 mm ²). - The GDLs have been preconditioned by 7 cycles of compression before starting.	
	2.5	29		
SGL 24 BC PTL	1.5	27.5	- The compressed area: 6 mm ² .	
	2.5	26		
SGL 24 BC MPL	1.5	15		
	2.5	14		
SGL 24 AA	1.5	9.6	This study: - The TLM method was used to determine the electrical contact resistance (gold-coated indenters were used).	This study: (TLM + gold covered indenters + cyclic compression)
	2.5	8.9		
SGL 24 BA	1.5	13.9	- A Dynamic Mechanical Analyser was used to apply the mechanical excitation (5 cycles of compression force of 0 to –65 N).	
	2.5	12.9		
SGL 24 BC PTL	1.5	36.9	- Every Sample was tested 3 times. The values are selected for the 1st loading cycle of the 3rd test.	
	2.5	31.8		
SGL 24 BC MPL	1.5	9.3	- The compressed area: 8 mm ² .	
	2.5	7.8		

(continued on next page)

Table 4 (continued)

GDL studied	Compression pressure Vs ρc		Method of measurement or estimation (in literature)	Ref.
	σ (MPa)	ρc (mOhm.cm ²)		
Toray H90	1.5	5.5		
	2.5	5.1		
Toray H120	1.5	5.6		
	2.5	4.8		

all the impacts of GDL composition. For example, the PTFE increased the electrical difference between cycles and decreased the mechanical one.

This work has been conducted under room temperature and humidity conditions. A possible extension to this study is to conduct the measurements inside an environmental chamber applying FC humidity and temperature conditions. The contact resistivities measured in this research can also be used in numerical models to evaluate the global contact resistance and the Ohmic losses regarding the pressure distribution on GDLs.

Declaration of competing interest

The authors declare that they have no known competing financial interests or personal relationships that could have appeared to influence the work reported in this paper.

CRediT authorship contribution statement

Khadidja Bouziane: Project administration, Investigation, Formal analysis, Writing - original draft, Writing - review & editing. **El Mahdi Khetabi:** Visualization, Writing - review & editing. **Rémy Lachat:** Conceptualization, Methodology, Writing - review & editing, Supervision. **Nada Zamel:** Writing - review & editing, Supervision. **Yann Meyer:** Conceptualization, Methodology, Validation, Writing - original draft, Writing - review & editing, Supervision. **Denis Candusso:** Conceptualization, Visualization, Validation, Writing - original draft, Writing - review & editing, Supervision.

Acknowledgements

The “Région Bourgogne-Franche-Comté” is gratefully acknowledged for its support through the ELICOP Project (Ref. 2015C-4944 and 2015-4948). The French “Ministère de l'Enseignement supérieur, de la Recherche et de l'Innovation” is gratefully acknowledged for the funding of Khadidja Bouziane's PhD Thesis (Contrat doctoral Univ. Paris Sud n°2017-225). In addition, the authors would like to gratefully acknowledge the Plastic Omnium Company for the support given to this research project.

References

- [1] W.R.W. Daud, R.E. Rosli, E.H. Majlan, S.A.A. Hamid, R. Mohamed, T. Husaini, PEM fuel cell system control: a review, *Renew. Energy* 113 (2017) 620–638, <https://doi.org/10.1016/j.renene.2017.06.027>.
- [2] S. Mekhilef, R. Saidur, A. Safari, Comparative study of different fuel cell technologies, *Renew. Sustain. Energy Rev.* 16 (2012) 981–989, <https://doi.org/10.1016/j.rser.2011.09.020>.
- [3] A. Kazim, Introduction of PEM fuel-cell vehicles in the transportation sector of the United Arab Emirates, *Appl. Energy* 74 (2003) 125–133, [https://doi.org/10.1016/S0306-2619\(02\)00138-1](https://doi.org/10.1016/S0306-2619(02)00138-1).
- [4] G. Giaccoppo, S. Hovland, O. Barbera, 2 kW Modular PEM fuel cell stack for space applications: development and test for operation under relevant conditions, *Appl. Energy* 242 (2019) 1683–1696, <https://doi.org/10.1016/j.apenergy.2019.03.188>.
- [5] D. Hart, F. Lehner, R. Rose, J. Lewis, M. Klippenstein, The fuel cell industry review, <http://www.fuelcellindustryreview.com/archive/TheFuelCellIndustryReview2017.pdf>, 2017 accessed 14 May 2019.
- [6] R. Salim, M. Nabag, H. Noura, A. Fardoun, The parameter identification of the Nexa 1.2 kW PEMFC's model using particle swarm optimization, *Renew. Energy* 82 (2015) 26–34, <https://doi.org/10.1016/j.renene.2014.10.012>.
- [7] J. Park, H. Oh, T. Ha, Y.I. Lee, K. Min, A review of the gas diffusion layer in proton exchange membrane fuel cells: durability and degradation, *Appl. Energy* 155 (2015) 866–880, <https://doi.org/10.1016/j.apenergy.2015.06.068>.
- [8] P. Pei, H. Chen, Main factors affecting the lifetime of Proton Exchange Membrane fuel cells in vehicle applications: a review, *Appl. Energy* 125 (2014) 60–75, <https://doi.org/10.1016/j.apenergy.2014.03.048>.
- [9] H. Zhang, X. Li, X. Liu, J. Yan, Enhancing fuel cell durability for fuel cell plug-in hybrid electric vehicles through strategic power management, *Appl. Energy* 241 (2019) 483–490, <https://doi.org/10.1016/j.apenergy.2019.02.040>.
- [10] A.D.J. Larminie, *Fuel Cell Systems Explained*, John Wiley & Sons, 2013.
- [11] A.M.B. Blunier, *Piles à combustible: Principes, modélisation, applications avec exercices et problèmes corrigés*, 2007.
- [12] E. Alizadeh, M.M. Barzegari, M. Momenifar, M. Ghadimi, S.H.M. Saadat, Investigation of contact pressure distribution over the active area of PEM fuel cell stack, *Int. J. Hydrogen Energy* 41 (2016) 3062–3071, <https://doi.org/10.1016/j.ijhydene.2015.12.057>.
- [13] Y. Hou, X. Zhang, X. Lu, D. Hao, L. Ma, P. Li, AC impedance characteristics of a vehicle PEM fuel cell stack under strengthened road vibrating conditions, *Int. J. Hydrogen Energy* 39 (2014) 18362–18368, <https://doi.org/10.1016/j.ijhydene.2014.09.054>.
- [14] C.J. Netwall, B.D. Gould, J.A. Rodgers, N.J. Nasello, K.E. Swider-Lyons, Decreasing contact resistance in proton-exchange membrane fuel cells with metal bipolar plates, *J. Power Sources* 227 (2013) 137–144, <https://doi.org/10.1016/j.jpowsour.2012.11.012>.
- [15] D. Ye, E. Gauthier, J.B. Benziger, M. Pan, Bulk and contact resistances of gas diffusion layers in proton exchange membrane fuel cells, *J. Power Sources* 256 (2014) 449–456, <https://doi.org/10.1016/j.jpowsour.2014.01.082>.
- [16] E. Alizadeh, M. Ghadimi, M.M. Barzegari, M. Momenifar, S.H.M. Saadat, Development of contact pressure distribution of PEM fuel cell's MEA using novel clamping mechanism, *Energy* 131 (2017) 92–97, <https://doi.org/10.1016/j.energy.2017.05.036>.
- [17] R. Banan, A. Bazylak, J. Zu, Combined effects of environmental vibrations and hygrothermal fatigue on mechanical damage in PEM fuel cells, *Int. J. Hydrogen Energy* 40 (2015) 1911–1922, <https://doi.org/10.1016/j.ijhydene.2014.11.125>.
- [18] A. Bates, S. Mukherjee, S. Hwang, S.C. Lee, O. Kwon, G.H. Choi, S. Park, Simulation and experimental analysis of the clamping pressure distribution in a PEM fuel cell stack, *Int. J. Hydrogen Energy* 38 (2013) 6481–6493, <https://doi.org/10.1016/j.ijhydene.2013.03.049>.
- [19] S. El Oualid, R. Lachat, D. Candusso, Y. Meyer, Characterization process to measure the electrical contact resistance of Gas Diffusion Layers under mechanical static compressive loads, *Int. J. Hydrogen Energy* 42 (2017) 23920–23931, <https://doi.org/10.1016/j.ijhydene.2017.03.130>.
- [20] P.A. Gigos, Y. Faydi, Y. Meyer, Mechanical characterization and analytical modeling of gas diffusion layers under cyclic compression, *Int. J. Hydrogen Energy* 40 (2015) 5958–5965, <https://doi.org/10.1016/j.ijhydene.2015.02.136>.
- [21] S.R. Dhanushkodi, F. Capitanio, T. Biggs, W. Mérida, Understanding flexural, mechanical and physico-chemical properties of gas diffusion layers for polymer membrane fuel cell and electrolyzer systems, *Int. J. Hydrogen Energy* 40 (2015) 16846–16859, <https://doi.org/10.1016/j.ijhydene.2015.07.033>.
- [22] S. Chevalier, N. Lavielle, B.D. Hatton, A. Bazylak, Novel electrospun gas diffusion layers for polymer electrolyte membrane fuel cells: Part I. Fabrication, morphological characterization, and in situ performance, *J. Power Sources* 352 (2017) 272–280, <https://doi.org/10.1016/j.jpowsour.2017.03.098>.
- [23] X. Xie, R. Wang, K. Jiao, G. Zhang, J. Zhou, Q. Du, Investigation of the effect of micro-porous layer on PEM fuel cell cold start operation, *Renew. Energy* 117 (2018) 125–134, <https://doi.org/10.1016/j.renene.2017.10.039>.
- [24] A. Forner-Cuenca, J. Biesdorf, L. Gubler, P.M. Kristiansen, T.J. Schmidt, P. Boillat, Engineered water highways in fuel cells: radiation grafting of gas diffusion layers, *Adv. Mater. Weinheim* 27 (2015) 6317–6322, <https://doi.org/10.1002/adma.201503557>.
- [25] D. Gerteisen, C. Sadeler, Stability and performance improvement of a polymer electrolyte membrane fuel cell stack by laser perforation of gas diffusion layers, *J. Power Sources* 195 (2010) 5252–5257, <https://doi.org/10.1016/j.jpowsour.2010.03.021>.
- [26] D. Gerteisen, T. Heilmann, C. Ziegler, Enhancing liquid water transport by laser perforation of a GDL in a PEM fuel cell, *J. Power Sources* 177 (2008) 348–354, <https://doi.org/10.1016/j.jpowsour.2007.11.080>.
- [27] J.H. Chun, D.H. Jo, S.G. Kim, S.H. Park, C.H. Lee, E.S. Lee, J.-Y. Jyoung, S.H. Kim,

- Development of a porosity-graded micro porous layer using thermal expandable graphite for proton exchange membrane fuel cells, *Renew. Energy* 58 (2013) 28–33, <https://doi.org/10.1016/j.renene.2013.02.025>.
- [28] M. Im Kong, J.W. Choi, S.I. Kim, E.S. Lee, M.S. Kim, Experimental study on the self-humidification effect in proton exchange membrane fuel cells containing double gas diffusion backing layer, *Appl. Energy* 145 (2015) 345–353, <https://doi.org/10.1016/j.apenergy.2015.02.027>.
- [29] M. Im Kong, A. Jung, M.S. Kim, Investigations on the double gas diffusion backing layer for performance improvement of self-humidified proton exchange membrane fuel cells, *Appl. Energy* 176 (2016) 149–156, <https://doi.org/10.1016/j.apenergy.2016.05.057>.
- [30] E.E. Kahveci, I. Taymaz, Experimental study on performance evaluation of PEM fuel cell by coating bipolar plate with materials having different contact angle, *Fuel* 253 (2019) 1274–1281, <https://doi.org/10.1016/j.fuel.2019.05.110>.
- [31] O.S. Burheim, G.A. Crymble, R. Bock, N. Hussain, S. Pasupathi, A. Du Plessis, S. Le Roux, F. Seland, H. Su, B.G. Pollet, Thermal conductivity in the three layered regions of micro porous layer coated porous transport layers for the PEM fuel cell, *Int. J. Hydrogen Energy* 40 (2015) 16775–16785, <https://doi.org/10.1016/j.ijhydene.2015.07.169>.
- [32] Y. Faydi, R. Lachat, Y. Meyer, Thermomechanical characterisation of commercial gas diffusion layers of a proton exchange membrane fuel cell for high compressive pre-loads under dynamic excitation, *Fuel* 182 (2016) 124–130, <https://doi.org/10.1016/j.fuel.2016.05.074>.
- [33] H. Sadeghifar, N. Djalili, M. Bahrami, Thermal conductivity of a graphite bipolar plate (BPP) and its thermal contact resistance with fuel cell gas diffusion layers: effect of compression, PTFE, micro porous layer (MPL), BPP out-of-flatness and cyclic load, *J. Power Sources* 273 (2015) 96–104, <https://doi.org/10.1016/j.jpowsour.2014.09.062>.
- [34] S. Prass, S. Hasanpour, P.K. Sow, A.B. Phillion, W. Mérida, Microscale X-ray tomographic investigation of the interfacial morphology between the catalyst and micro porous layers in proton exchange membrane fuel cells, *J. Power Sources* 319 (2016) 82–89, <https://doi.org/10.1016/j.jpowsour.2016.04.031>.
- [35] A.H. Mahmoudi, A. Ramiar, Q. Esmaili, Effect of inhomogeneous compression of gas diffusion layer on the performance of PEMFC with interdigitated flow field, *Energy Convers. Manag.* 110 (2016) 78–89, <https://doi.org/10.1016/j.enconman.2015.12.012>.
- [36] H. Ishikawa, T. Teramoto, Y. Ueyama, Y. Sugawara, Y. Sakiyama, M. Kusakabe, K. Miyatake, M. Uchida, Use of a sub-gasket and soft gas diffusion layer to mitigate mechanical degradation of a hydrocarbon membrane for polymer electrolyte fuel cells in wet-dry cycling, *J. Power Sources* 325 (2016) 35–41, <https://doi.org/10.1016/j.jpowsour.2016.06.012>.
- [37] G.M. Domínguez Almaraz, J.A. Ruiz Vilchez, A. Domínguez, Y. Meyer, Ultrasonic fatigue endurance of thin carbon fiber sheets, *Metall. Mater. Trans.* 47 (2016) 1654–1660, <https://doi.org/10.1007/s11661-016-3350-9>.
- [38] N. Ul Hassan, M. Kilic, E. Okumus, B. Tunaboylu, A.M. Soydan, Experimental determination of optimal clamping torque for AB-PEM Fuel cell, *J. Electrochem. Sci. Eng.* 6 (2016) 9, <https://doi.org/10.5599/jese.198>.
- [39] D. Singdeo, T. Dey, P.C. Ghosh, Contact resistance between bipolar plate and gas diffusion layer in high temperature polymer electrolyte fuel cells, *Int. J. Hydrogen Energy* 39 (2014) 987–995, <https://doi.org/10.1016/j.ijhydene.2013.10.147>.
- [40] M.S. Ismail, D.B. Ingham, L. Ma, M. Pourkashanian, The contact resistance between gas diffusion layers and bipolar plates as they are assembled in proton exchange membrane fuel cells, *Renew. Energy* 52 (2013) 40–45, <https://doi.org/10.1016/j.renene.2012.10.025>.
- [41] C.-H. Chien, Y.-L. Hu, T.-H. Su, H.-T. Liu, C.-T. Wang, P.-F. Yang, Y.-X. Lu, Effects of bolt pre-loading variations on performance of GDL in a bolted PEMFC by 3-D FEM analysis, *Energy* 113 (2016) 1174–1187, <https://doi.org/10.1016/j.energy.2016.07.075>.
- [42] K.D. Baik, S.I. Kim, B.K. Hong, K. Han, M.S. Kim, Effects of gas diffusion layer structure on the open circuit voltage and hydrogen crossover of polymer electrolyte membrane fuel cells, *Int. J. Hydrogen Energy* 36 (2011) 9916–9925, <https://doi.org/10.1016/j.ijhydene.2011.05.088>.
- [43] Ö. Aydin, M. Zedda, N. Zamel, U. Groos, C. Hebling, Comprehensive understanding of electrical conductivity measurements of gas diffusion media of PEM fuel cells, in: 20th World Hydrogen Energy Conference (WHEC 2014): Gwangju, South Korea, 15–20 June 2014, Committee of WHEC, Gwangju, South Korea, 2014.
- [44] Ö. Aydin, M. Zedda, N. Zamel, Challenges associated with measuring the intrinsic electrical conductivity of carbon paper diffusion media, *Fuel Cell* 15 (2015) 537–544, <https://doi.org/10.1002/fuce.201400125>.
- [45] M. Ahmad, R. Harrison, J. Meredith, A. Bindel, B. Todd, Validation of a fuel cell compression spring equivalent model using polarisation data, *Int. J. Hydrogen Energy* 42 (2017) 8109–8118, <https://doi.org/10.1016/j.ijhydene.2017.01.216>.
- [46] M. Hamour, J.C. Grandidier, A. Oubrahim, S. Martemianov, Electrical conductivity of PEMFC under loading, *J. Power Sources* 289 (2015) 160–167, <https://doi.org/10.1016/j.jpowsour.2015.04.145>.
- [47] T.J. Mason, J. Millichamp, P.R. Shearing, D.J.L. Brett, A study of the effect of compression on the performance of polymer electrolyte fuel cells using electrochemical impedance spectroscopy and dimensional change analysis, *Int. J. Hydrogen Energy* 38 (2013) 7414–7422, <https://doi.org/10.1016/j.ijhydene.2013.04.021>.
- [48] M. Zhiani, S. Kamali, S. Majidi, In-plane gas permeability and thought-plane resistivity of the gas diffusion layer influenced by homogenization technique and its effect on the proton exchange membrane fuel cell cathode performance, *Int. J. Hydrogen Energy* 41 (2016) 1112–1119, <https://doi.org/10.1016/j.ijhydene.2015.10.052>.
- [49] E.M. Khetabi, K. Bouziane, N. Zamel, X. François, Y. Meyer, D. Candusso, Effects of mechanical compression on the performance of polymer electrolyte fuel cells and analysis through in-situ characterisation techniques - a review, *J. Power Sources* 424 (2019) 8–26, <https://doi.org/10.1016/j.jpowsour.2019.03.071>.
- [50] N. Zamel, X. Li, J. Shen, Numerical estimation of the effective electrical conductivity in carbon paper diffusion media, *Appl. Energy* 93 (2012) 39–44, <https://doi.org/10.1016/j.apenergy.2011.08.037>.
- [51] M.S. Ismail, K.J. Hughes, D.B. Ingham, L. Ma, M. Pourkashanian, Effects of anisotropic permeability and electrical conductivity of gas diffusion layers on the performance of proton exchange membrane fuel cells, *Appl. Energy* 95 (2012) 50–63, <https://doi.org/10.1016/j.apenergy.2012.02.003>.
- [52] M.S. Ismail, T. Damjanovic, D.B. Ingham, M. Pourkashanian, A. Westwood, Effect of polytetrafluoroethylene-treatment and microporous layer-coating on the electrical conductivity of gas diffusion layers used in proton exchange membrane fuel cells, *J. Power Sources* 195 (2010) 2700–2708, <https://doi.org/10.1016/j.jpowsour.2009.11.069>.
- [53] D. Todd, S. Bennett, W. Mérida, Anisotropic electrical resistance of proton exchange membrane fuel cell transport layers as a function of cyclic strain, *Int. J. Hydrogen Energy* 41 (2016) 6029–6035, <https://doi.org/10.1016/j.ijhydene.2016.02.111>.
- [54] D. Qiu, H. Janßen, L. Peng, P. Irmscher, X. Lai, W. Lehnert, Electrical resistance and microstructure of typical gas diffusion layers for proton exchange membrane fuel cell under compression, *Appl. Energy* 231 (2018) 127–137, <https://doi.org/10.1016/j.apenergy.2018.09.117>.
- [55] T.J. Mason, J. Millichamp, T.P. Neville, A. El-kharouf, B.G. Pollet, D.J.L. Brett, Effect of clamping pressure on ohmic resistance and compression of gas diffusion layers for polymer electrolyte fuel cells, *J. Power Sources* 219 (2012) 52–59, <https://doi.org/10.1016/j.jpowsour.2012.07.021>.
- [56] A. Miyazawa, T. Himeno, A. Nishikata, Electrical properties of bipolar plate and gas diffusion layer in PEFC, *J. Power Sources* 220 (2012) 199–204, <https://doi.org/10.1016/j.jpowsour.2012.07.127>.
- [57] A. El-kharouf, T.J. Mason, D.J.L. Brett, B.G. Pollet, Ex-situ characterisation of gas diffusion layers for proton exchange membrane fuel cells, *J. Power Sources* 218 (2012) 393–404, <https://doi.org/10.1016/j.jpowsour.2012.06.099>.
- [58] X. Lai, D.-a. Liu, L. Peng, J. Ni, A mechanical-electrical finite element method model for predicting contact resistance between bipolar plate and gas diffusion layer in PEM fuel cells, *J. Power Sources* 182 (2008) 153–159, <https://doi.org/10.1016/j.jpowsour.2008.03.069>.
- [59] L. Zhang, Y. Liu, H. Song, S. Wang, Y. Zhou, S.J. Hu, Estimation of contact resistance in proton exchange membrane fuel cells, *J. Power Sources* 162 (2006) 1165–1171, <https://doi.org/10.1016/j.jpowsour.2006.07.070>.
- [60] P. Zhou, P. Lin, C.W. Wu, Z. Li, Effect of nonuniformity of the contact pressure distribution on the electrical contact resistance in proton exchange membrane fuel cells, *Int. J. Hydrogen Energy* 36 (2011) 6039–6044, <https://doi.org/10.1016/j.ijhydene.2011.01.080>.
- [61] Fuel cell store, Toray carbon fiber paper “TGP-H”. <https://www.fuelcellsetc.com/store/DS/Toray-Paper-TGP-H-Datasheet.pdf> accessed 14 May 2019.
- [62] Fuel cell store, FREUDENBERG gas diffusion layers for PEMFC and DMFC. <http://www.fuelcellstore.com/spec-sheets/freudenberg-gdl-technical-data.pdf>.
- [63] G. Tuttle, Contact resistance and TLM measurements. http://tuttle.merc.iastate.edu/ee432/topics/metals/tlm_measurements.pdf accessed 14 May 2019.
- [64] W. Shockley, Research and Investigation of Inverse Epitaxial UHF Power Transistors: A1-TOR-64-20, Wright-Patterson Air Force Base, USA, 1964.
- [65] D.K. Schroder, Semiconductor Material and Device Characterization, John Wiley & Sons, Inc, Hoboken, NJ, USA, 2005.
- [66] H. Murrmann, D. Widmann, Current crowding on metal contacts to planar devices, *IEEE Trans. Electron. Dev.* 16 (1969) 1022–1024, <https://doi.org/10.1109/T-ED.1969.16904>.
- [67] H. Murrmann, D. Widmann, Messung des Übergangswiderstandes zwischen Metall und Diffusionsschicht. Si-Planarelementen, *Solid State Electron.* 12 (1969) 879–886.
- [68] H.H. Berger, Contact resistance and contact resistivity, *J. Electrochem. Soc.* 119 (1972) 507, <https://doi.org/10.1149/1.2404240>.
- [69] Joint Committee for Guides in Metrology, Evaluation of measurement data — guide to the expression of uncertainty in measurement. https://www.bipm.org/utils/common/documents/jcgm/JCGM_100_2008_E.pdf, September 2008 accessed 23 January 2020.
- [70] A. El-kharouf, R. Steinberger-Wilckens, The effect of clamping pressure on gas diffusion layer performance in polymer electrolyte fuel cells, *Fuel Cell* 15 (2015) 802–812, <https://doi.org/10.1002/fuce.201500088>.